COMBINATORIAL METHOD TO OPTIMIZE

OXYGEN DIFFUSION OF $(La_{1-x}Sr_x)_{1-y}CoO_3$

FOR SOFC CATHODES

by

Peter Bocchini

A thesis submitted to the Faculty of the University of Delaware in partial fulfillment of the requirements for the degree of Honors Bachelor of Mechanical Engineering with Distinction.

Spring 2010

COMBINATORIAL METHOD TO OPTIMIZE

OXYGEN DIFFUSION OF $(La_{1-x}Sr_x)_{1-y}CoO_3$

FOR SOFC CATHODES

by

Peter Bocchini

Approved: _____

Joshua Hertz, Ph.D.
Professor in charge of thesis on behalf of the Advisory Committee

Approved: _____

Ajay Prasad, Ph.D.
Committee member from the Department of Mechanical Engineering

Approved: _____

Victor Kaliakin, Ph.D.
Committee member from the Board of Senior Thesis Readers

Approved: _____

Alan Fox, Ph.D.
Director, University Honors Program

ACKNOWLEDGMENTS

There are multiple people that I would like to acknowledge and thank for playing important roles in supporting my ability and desire to conduct research. I would first like to thank **Dr. Ajay Prasad** who gave me my first research experience, and **Srikanth Arisetty** for guiding me during this experience. I would also like to acknowledge **Dr. Albert Davydov** for further mentoring me at NIST. Lastly for my scientific advisors, I would especially like to thank **Dr. Joshua Hertz** for allowing me to work in his lab which allowed me to produce this paper.

I'd like to thank Hertz Group members **Andrew Baker** and **James White** for their aid throughout my research. Also to **Dr. Tom Beebe** and **Holt Bui** who generously gave their time and equipment for SIMS measurements. **Steve Beard** should also be thanked not only for his guidance in the machine shop but also his unrivaled patience after I had broken several of his mill bits.

Most importantly, I'd like to thank my family for all of the support they've given me throughout my life. Specifically my mother, **Pier Bocchini**, for making sure I always did well in school and who gave me the resources to do so, my father, **Perry Bocchini**, for trying to not let me get too overwhelmed, and my grandparents who have done nothing but encourage me.

TABLE OF CONTENTS

LIST OF FIGURES

ABSTRACT

Environmental issues paired with increased concern over energy security have made a need for energy efficient and non-carbon fueled power. This study has set the foundation for a novel way to choose materials and material compositions with optimal oxygen diffusion properties for cathodes in solid oxide fuel cells (SOFCs).

SOFCs are one of the most promising types of fuel cells, being able to generate high efficiency stationary power. SOFCs can run on both hydrogen and hydrocarbon fuels such as natural gas. The ability to use multiple fuel types makes SOFCs ideal for the transition from a fossil fuel based system to a greener hydrogen economy. While SOFCs have been widely studied, there has been no specific standards for their cathode material (other than that they have a perovskite crystal structure). The major function of the cathode is to conduct electrons and provide oxygen ions to the electrolyte. This thesis has laid out a quick and efficient method by which the oxygen diffusion properties of a library of perovskite materials can be tested.

This thesis utilized sputtering to create a thin film with varying compositions along the same substrate. Secondary Ion Mass Spectrometry (SIMS) was used to characterize the composition of the films and ensure that a variety of compositions were present on the substrate. This study focused on $(La_{1-x}Sr_x)_{1-y}CoO_3$ however the method described would be valid for any perovskite material. Furthermore, while this research was done mainly to develop a way to test materials

for fuel cell use, perovskites have been shown to have a wide variety of applications which allows this study to be relevant to other areas of research.

Chapter 1

INTRODUCTION AND BACKGROUND

1.1 Fuel Cell Relevance

Recent concern about global climate change and the world's overconsumption of energy has lead to an increased need for efficient and environmentally neutral energy technologies. As fuel cell technology improves, they are becoming more viable power producers for the future. Fuel cells benefit from their high efficiency and can be fueled by hydrogen to produce only water as a byproduct. There are many different types of fuel cells which use various fuels, materials, and designs. Of these, one of the most promising is the solid oxide fuel cell (SOFC). SOFCs can be fueled by both hydrogen and fossil fuels. This allows for a smooth transition from a carbon emitting society to a greener hydrogen economy.

1.2 Benefits of SOFCs

Solid oxide fuel cells have many advantages over both conventional combustion methods and other types of fuel cells. SOFC systems are most often designed for stationary power applications and are typically compared to natural gas generators for viability analysis. A SOFC system can reach efficiencies between 40-60%, whereas conventional generators top out at around 35%. This discrepancy occurs because while heat engines are limited by the Carnot efficiency limit, fuel cells create energy by electrochemical means and have an efficiency ceiling much higher than heat engines. Increased efficiency can significantly impact pollution production. Unlike the

more widely publicized polymer membrane based fuel cells (PEMFCs), SOFCs are not limited to being fueled by hydrogen and can run on hydrocarbons such as natural gas. Meier et al. estimates that 454 tonnes of CO_2 are released per GWh of energy when combusting natural gas. Using a very reasonable SOFC efficiency of 50%, converting natural gas to energy through a fuel cell will produce 318 tonnes of CO_2 per GWh. That is a reduction of 136 tonnes of CO_2. Additionally if green hydrogen is used to fuel the SOFC systems, the power is almost entirely environmentally neutral. While the most common way to produce hydrogen still involves extraction from fossil fuels, there has been a continuous growth in research to finding ways to produce hydrogen from renewable sources which will make fuel cells even more advantageous.

SOFCs also have traits that allow them to be more desirable than other fuel cell types, especially for stationary applications. These benefits stem mainly from SOFCs ability to operate at high temperatures, usually between 600°C and 1000°C. Due to material constraints, PEMFCs are limited to temperatures below about 90°C. Chemical reaction kinetics are more rapid at higher temperatures and, as fuel cells are powered by chemical reactions, higher operating temperatures are often desirable. To make up for lower operating temperatures, PEMFC utilize platinum catalysts which speed up the reaction but have the negative effect of adding additional material expenses. SOFCs are able to use low cost nickel catalysts. Another benefit of SOFCs is that while most other types of fuel cells can only run on hydrogen, SOFCs have the ability to internally reform hydrocarbons. This feature allows for the same hydrocarbons that would normally be combusted, to be electrochemically reacted in a fuel cell system with higher efficiency. The high temperatures of the SOFC also allow for unique hybrid systems to be made by adding a bottoming cycle to the fuel cell

(Larminie 2003). For this method, a steam or gas turbine is powered by the waste heat of the fuel cell and allows for greater overall efficiency.

1.3 Oxygen Diffusion and Chemistry

The necessity for a high rate of oxygen diffusion can be shown by the chemical reactions at the anode and cathode. Figure 1.1 illustrates that, unlike polymer fuel cells where the proton ion promotes the reaction cycle, it is actually the oxygen ion which crosses the electrolyte to react and release the electrons. Hydrogen must be pumped from a supply tank into the system. The O_2 can also be pumped from a tank, however a more practical method is to supply the O_2 through the air. In either case, the cathode oxygen reaction is the major limiting agent to the fuel cell's power output. Thus, oxygen diffusivity is a property of the utmost importance for the SOFC cathode material. A more diffusive cathode allows for a higher O_2 concentration which allows for better oxygen availability and higher power which increases efficiency and overall performance.

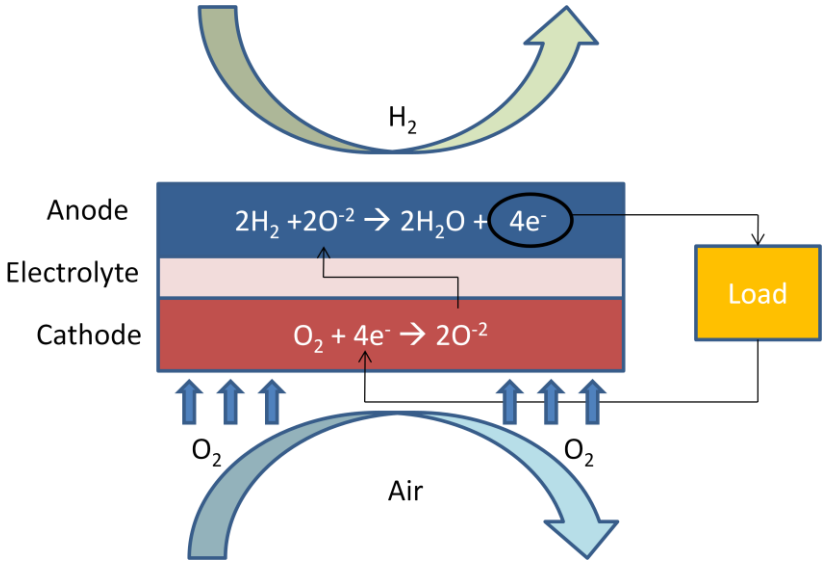

Figure 1.1: SOFC Diagram

1.4 Oxygen Conducting Perovskite Materials

The perovskite crystal structure is of the form ABO_3. Materials containing a perovskite crystal structure have been shown to exhibit a wide variety of desirable electrical, thermal, and catalytic properties. The perovskite structure can also be utilized to create high rate oxygen diffusers. This is done by doping the A site with ions of a lower valence. For this study $(La_{1-x}\,Sr_x)_{1-y}CoO_3$ will be the perovskite structure being examined. The reasons for choosing $(La_{1-x}\,Sr_x)_{1-y}CoO_3$ is that first, it is a common material being studied for SOFC cathodes and is a known oxygen conductor and second, $(La_{1-x}\,Sr_x)_{1-y}CoO_3$ is a relatively easy perovskite structure to synthesize because it only has three major components. In this case the original perovskite material is $LaCoO_3$. The A site is occupied by La^{+3} and the B site is occupied by Co^{+3}. Sr^{+2} is used as a dopant and takes the place of the La^{+3} which causes a charge imbalance. Charge neutrality is realized by oxygen leaving the lattice thus creating oxygen vacancies (Rossiny 2008). The vacancies allow oxygen to flow through the material. At low to moderate concentrations, increasing the number of vacancies leads to higher rates of oxygen diffusion.

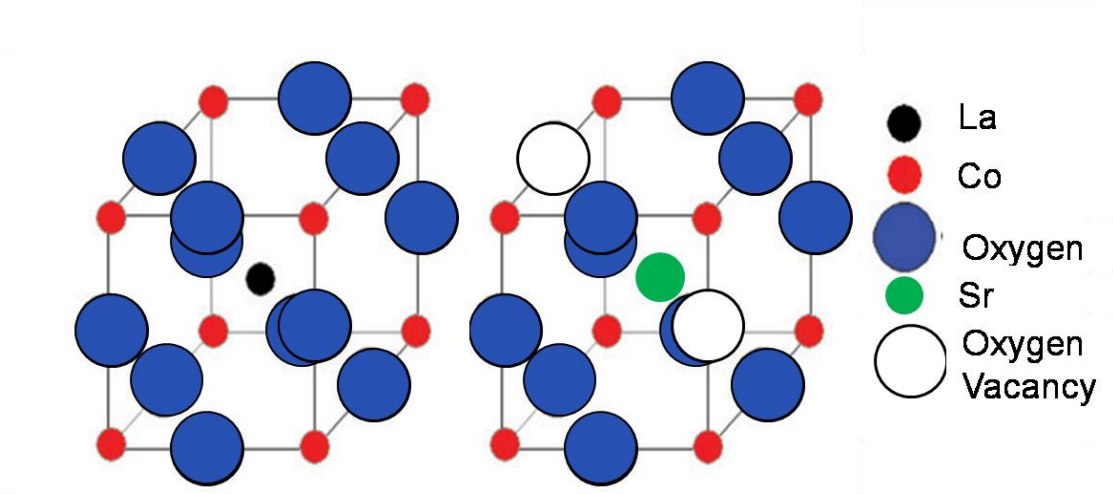

Figure 1.2: Perovskite Crystal Structure (Modified from U. of Cambridge, 2006)

1.5 Importance of Combinatorial Approach

While perovskite materials have been studied for many applications, the diffusion properties of many compositions of perovskite materials are unknown. This is mostly due to constraints on the time necessary to produce a ceramic of proper composition and crystal structure. Conventional methods to produce perovskite materials for testing are very time consuming. These methods typically involve making a bulk sample of the ceramic which can take upwards of a week for only a single composition. An example relating to this study is that whereas $La_{0.5}Sr_{0.5}CoO_3$ and $La_{0.8}Sr_{0.2}CoO_3$ have been studied extensively, the properties of other compositions of $(La_{1-x}Sr_x)_{1-y}CoO_3$ are relatively undocumented. As material properties can differ significantly based on composition, being able to identify these varying properties is valuable. This work has produced the framework for studying the oxygen diffusion properties of pervoskite materials in a much quicker and extensive way. The

combinatorial approach allows for a wide variety of compositions. Figure 1.3 represents the compositional distribution along a 75 mm silicon substrate. Each dot represents a slightly varying composition. All compositions can be analyzed in parallel which drastically reduces experimental time while simultaneously increasing the comprehensiveness of the data for the material.

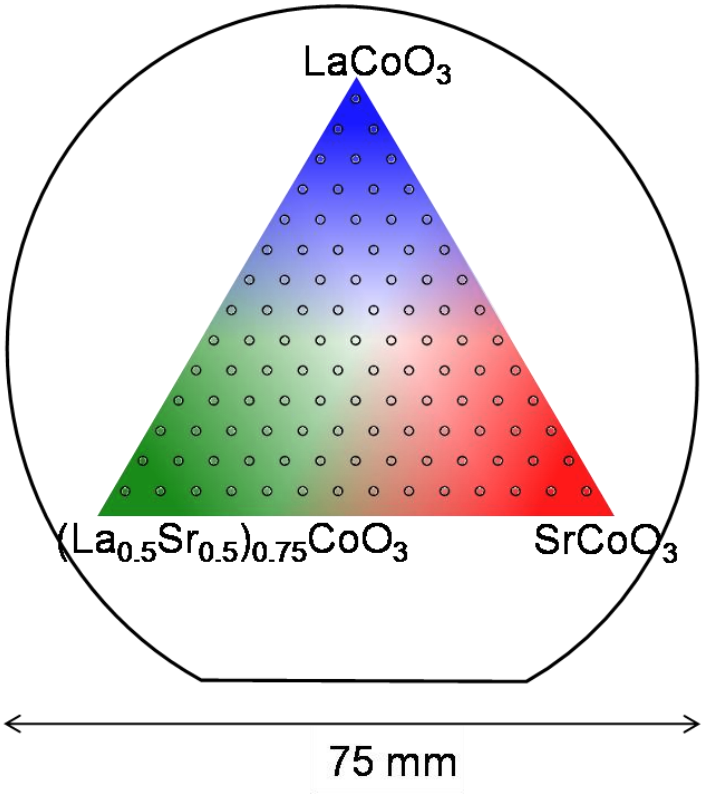

Figure 1.3: Example of Compositional Distribution on Substrate

Chapter 2

METHODS

2.1 Methods Overview

The process being performed for this oxygen diffusion study is comprised of various methods. Sputtering targets were made using a mixed powder and press method. X-ray diffraction was used to find the crystal structure of the various sputter targets. Sputtering trials were executed at multiple conditions to find the deposition rate of each target. The diffusion equation and diffusion coefficients of known values of $(La_{1-x}Sr_x)_{1-y}CoO_3$ were used to get a general baseline for the time and temperature that oxygen diffusion experiments should be conducted. The differential equation for diffusion through a semi-infinite solid has been solved by Crank which will be reviewed below. The deposition rate allowed a film of appropriate size, as defined from the diffusion equation, to be created for testing. After finding the deposition rates of each target a combinatorial film of various compositions of $(La_{1-x}Sr_x)_{1-y}CoO_3$ was created which was then annealed in an oxygen diffusion chamber in a ^{16}O rich environment. The oxygen diffusion chamber was designed and fabricated during the sputtering experiments. Secondary Ion Mass spectrometry was used to measure the composition of the film to find the distribution along the substrate.

2.2 Sputtering

Sputtering is a thin film fabrication technique by which a target material is bombarded with energized atoms from a plasma that causes the target atoms to be ejected from the bulk material and coat a given substrate. The three major variables

which affect the deposition rate are the power fed into the target, operating pressure, and gas composition. All operating conditions were varied for the deposition rate measurements.

2.2.1 Target Making

The first step in performing the sputtering process was to create the targets necessary to give the required compositions. These targets were made by mixing powders of various compositions. In the case of this study, three targets are needed to be sputtered simultaneously to create a diverse set of compositions of $(La_{1-x}\,Sr_x)_{1-y}CoO_3$. The three desired targets are $LaCoO_3$, $SrCoO_3$, and $(La_{0.5}Sr_{0.5})_{0.75}CoO_3$. The following powders and amounts were used to create the desired targets:

$LaCoO_3$: La_2O_3, Co_3O_4

$$x\ grams\ LaCoO_3 * \left(\frac{1\ mol\ LaCoO_3}{246\ grams}\right) \begin{cases} \left(\frac{1\ mol\ Co}{1\ mol\ LaCoO_3}\right) * \left(\frac{1\ mol\ Co_3O_4}{3\ mol\ Co}\right) * \left(\frac{241\ grams\ Co_3O_4}{1\ mol\ Co_3O_4}\right) \\ \left(\frac{1\ mol\ La}{1\ mol\ LaCoO_3}\right) * \left(\frac{1\ mol\ La_2O_3}{2\ mol\ Co}\right) * \left(\frac{326\ grams\ La_2O_3}{1\ mol\ La_2O_3}\right) \end{cases}$$

Amount of powders needed:

$$x\ grams * 0.662\ La_2O_3$$

$$x\ grams * 0.327\ Co_3O_4$$

$SrCoO_3$: $SrCO_3$, Co_3O_4

$$x\ grams\ SrCoO_3 * \left(\frac{1\ mol\ SrCoO_3}{194.6\ grams}\right) \rightarrow \left(\frac{1\ mol\ Sr}{1\ mol\ SrCoO_3}\right) * \left(\frac{1\ mol\ SrCO_3}{1\ mol\ Sr}\right) * \left(\frac{148\ grams\ SrCO_3}{1\ mol\ SrCO_3}\right)$$

$$x\ grams\ SrCoO_3 * \left(\frac{1\ mol\ SrCoO_3}{194.6\ grams}\right) \rightarrow \left(\frac{1\ mol\ Co}{1\ mol\ SrCoO_3}\right) * \left(\frac{1\ mol\ Co_3O_4}{3\ mol\ Co}\right) * \left(\frac{241\ grams\ Co_3O_4}{1\ mol\ Co_3O_4}\right)$$

Amount of powders needed:

$$x\ grams * 0.758\ SrCO_3$$

$$x\ grams * 0.413\ Co_3O_4$$

$(La_{0.5}Sr_{0.5})_{0.75}CoO_3$: La_2O_3, $SrCO_3$, Co_3O_4

$$x\ grams\ La_{0.375}Sr_{0.375}CoO_3 * \left(\frac{1\ mol\ La_{.375}Sr_{.375}CoO_3}{192\ grams}\right) \rightarrow \left(\frac{0.375\ mol\ Sr}{1\ mol\ La_{0.375}Sr_{0.375}CoO_3}\right) * \left(\frac{1\ mol\ mol\ SrCO_3}{1\ mol\ Sr}\right) * \left(\frac{148\ grams\ SrCO_3}{1\ mol\ SrCO_3}\right)$$

$$x\ grams\ La_{0.375}Sr_{0.375}CoO_3 * \left(\frac{1\ mol\ La_{.375}Sr_{.375}CoO_3}{192\ grams}\right) \rightarrow \left(\frac{0.375\ mol\ La}{1\ mol\ La_{0.375}Sr_{0.375}CoO_3}\right) * \left(\frac{1\ mol\ La_2O_3}{2\ mol\ Co}\right) * \left(\frac{326\ grams\ La_2O_3}{1\ mol\ La_2O_3}\right)$$

$$x\ grams\ La_{0.375}Sr_{0.375}CoO_3 * \left(\frac{1\ mol\ La_{.375}Sr_{.375}CoO_3}{192\ grams}\right) \rightarrow \left(\frac{1\ mol\ Co}{1\ mol\ La_{0.375}Sr_{0.375}CoO_3}\right) * \left(\frac{1\ mol\ Co_3O_4}{3\ mol\ Co}\right) * \left(\frac{241\ grams\ Co_3O_4}{1\ mol\ Co_3O_4}\right)$$

Amount of powders needed:

$$x\ grams * 0.288 SrCO_3$$

$$x\ grams * 0.318\ La_2O_3$$

$$x\ grams * 0.418\ Co_3O_4$$

Once the powders had been mixed to the desired amount, they needed to be ball milled to create a uniform mixture. During this process, plastic containers were filled with YSZ (Yttria Stabilized Zirconia) pellets which serve to uniformly mix the powders during tumbling. The powder was then poured into the container which was then filled

with deionized (DI) water. The container was capped and put into a tumbler for 24 hours to ensure the powders were well mixed. After mixing was complete, the ceramic slurry was strained to remove YSZ and placed on a hot plate to evaporate the water leaving a well mixed powder. The powder had to be placed in a furnace to be calcined so that the proper phase transformations could occur and a perovskite crystal structure was obtained. The powder was calcined at 1350 °C for 8 hours. After having cooled, a small powder sample was taken for X-ray diffraction (XRD) measurements to check that a suitable phase had been reached. The remaining powder was then prepared for pressing. This was done by adding 1 wt % polyvinyl alcohol (PVA) to the calcined powder. The PVA helps to hold the powder so that the shape after pressing is maintained. The PVA burns off in later heating so that the compositions of the targets were not altered. The calcined powders were ball-milled again to mix in the PVA as well as too break up any large pieces of ceramic that may have formed during calcining. The new slurry was again placed on a hot plate where it was left to dry. The resulting powder was then hand crushed using a pestle. The powder was then ready for pressing. This was done using an in-house mold. The mold comes in four parts, 2 pressing surfaces which are solid aluminum cylinders and 2 guiding surfaces which are aluminum tubing and hold the pressing surfaces in line. The mold makes targets 3 inches in diameter. Figure 2.1 below shows the mold. In preparation for pressing all surfaces of the mold were cleaned with acetone, isopropanol, and DI water. The surfaces were then coated with stearic acid which served as a lubricant. The powder was placed in the mold and was then pressed by a pneumatic uniaxial press to 5000 psi for 1 minute. The resulting targets looked somewhat like a hockey puck in appearance. Care was still needed to handle the targets as they remain fragile until further heating.

The targets were sintered to become stable robust ceramics. This was done by placing the targets in the furnace to a temperature of 1350°C. This process was done gradually so that thermal stresses would not develop and the targets would not break. The heating occurred as follows: 50°C/hr up to 300°C, 10°C/hr up to 500°C, 50°C/hr to 1350°C, and 100°C/hr back down to 0°C. The especially slow heating between 300 and 500°C was done because the PVA oxidizes between these temperatures. Rapid gas evolution as the PVA breaks down could have led to structural instability and cracking of the targets. The heating took place in an environment of pure O_2 so that impurities from the air would not react with the targets and so that the targets would not reduce (lose oxygen) at high temperature. Once removed from the furnace, the targets were suitable to use in the sputtering machine. A finished target can be seen in figure 2.2.

Figure 2.1: Target Mold

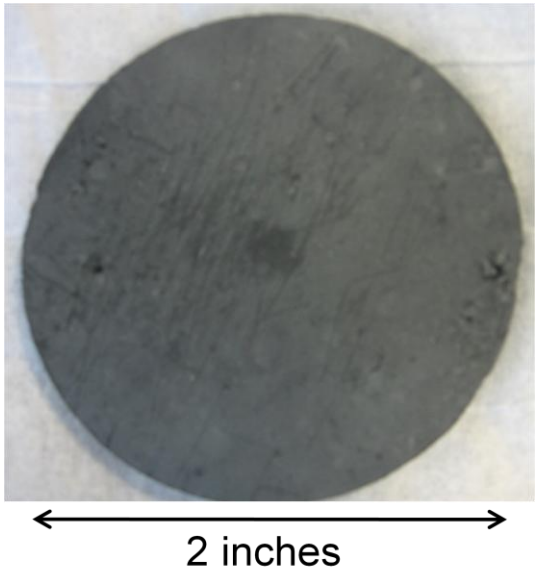

Figure 2.2: Finished Target

2.2.2 Deposition Rate

Before beginning the process of creating a combinatorial film, the deposition rates of each individual target needed to be obtained. The deposition rates are important for two major reasons. The first is that to create the proper compositional variation on the substrate, the deposition rates should be approximately the same. This ensures that a wide variety of compositions will be made and that one target does not dominate the film. The other reason is that film thickness is critical to the success of this project. Knowing the deposition rate of each individual target allows one to control the overall thickness of the film.

Deposition rate can be controlled by altering variables in the sputtering process. During this experiment the gas composition in the sputtering machine was a mix of O_2 and argon. The argon gas ionizes and becomes a plasma. By increasing the ratio of argon to O_2, more gas is available to be ionized and therefore allows more

argon atoms to ionize which leads to a higher rate of bombardment into the desired target thus causing more target material to be shot onto the substrate. Another method for increasing the sputter rate is to lower the overall system pressure. Atoms are statistically bound in how far they can travel by their mean free path, that is, the average distance an atom can travel without colliding into another atom. Reducing the pressure increases the mean free path of the atoms and allows the target material to have a more direct path to the substrate. The third way in which deposition rates can be altered is by varying the voltage to the target. The voltage supplies power which allows the argon to ionize. By increasing the power, more energy is sent into the plasma which again creates more collisions and causes more sputtering material to be deposited.

Desirable sputter rates were obtained by testing a variety of conditions. The sputtering system used has three guns. It is necessary to test the sputter rate of all three guns and targets and not assume that the same conditions will yield the same result for all targets. Deposition rate under the same conditions will vary from different target materials. The guns must also be tested because they are not all the same. Two of the guns are RF (radio frequency) and one is DC (direct current). The RF guns sputter at a lower rate than the DC gun. Sputter time was held constant at 3 hours for all trials. Variations in gas composition was altered between 4:1 $Ar:O_2$ and 9:1 $Ar:O_2$. Power was tested at 25 and 50 W. These wattages are relatively low for sputtering however due to the inherent brittleness and mechanical instability of the targets, higher powers were not used to avoid breaking the targets. Operating pressure varied between 10 and 20 mTorr.

After the deposition rates for the various sputter conditions had been logged. The settings were tweaked so that the deposition rate of each individual target was approximately the same. This ensures a wide variety of compositions on the film. The combinatorial film was then created by co-sputtering all three targets onto a 4 inch diameter silicon substrate for a time of 30 hours.

2.3 Oxygen Diffusion Chamber

2.3.1 Purpose of Diffusion Chamber

As will be talked about in more detail in section 2.5, an oxygen isotope exchange is necessary to measure the oxygen diffusion properties of the thin film. ^{16}O is the most abundant form of oxygen on earth, however ^{18}O is commercially available. It is reasonable to assume that the oxygen in perovskite film is comprised entirely of ^{16}O, and therefore oxygen diffusivity can be determined by annealing the film in an ^{18}O rich environment. The ratio of ^{18}O to ^{16}O can be measured via SIMS depth profiling. Creating an ^{18}O rich environment requires a high temperature closed volume container. The design process for the oxygen diffusion chamber is discussed below.

2.3.2 Chamber Design

The lab furnace had previously been equipped to flow in gas through metal fittings. While this setup works for flowing in large gas supplies such as in sintering process, the cost of ^{18}O is too high to flow through at such large volumes. This led for the need to fabricate a closed volume oxygen diffusion chamber that could be placed inside of the furnace. There were several key constraints that had to be addressed to ensure a successful design. The chamber must be made out of a material that can withstand high temperatures up to at least 800°C. The material must also be

creep resistant so that it does not bend and break during the annealing process. Lastly, the material should be thermal shock resistant. This led to two different design paths caused by the material choice between quartz and stainless steel. The concepts for quartz and one for stainless steel are discussed below.

The main challenge that needed to be addressed was how to enclose the samples in the chamber while also keeping it vacuum tight so that no gas could leak out and no air could leak in. The first quartz concept was to have the Brown Lab glass blower enclose the film inside of a closed tube then fill the container with ^{18}O after which the container would then be sealed. The major benefits of this design are that it creates very little internal volume. This would save the amount of gas needed to be used which will allow for more experiments to be run while simultaneously cutting experimental costs significantly. The major drawback of this type of design was that the only way to retrieve the samples post experiment was to break the quartz container. Running multiple experiments would have required that a new glass container be made for each individual experiment.

The second quartz concept tried to combat the need to be constantly remaking oxygen exchange vessels. The design consists of two sections. Section 1 is made up of a quartz tube that has been closed at one end. The other end will be fitted with a spherical glass socket joint. Section 2 consists of an O-ring ball joint on one end. The other end consists of a double bore stopcock which will allows for a vacuum pump to be attached to one of the fittings and ^{18}O and ^{16}O to be attached to the other. The samples would be placed in section 1 then a clamp would be used to hold the two sections together at the joint. A sketch of this can be found in figure 2.4 below. The ball and socket joint allows for easy access to the samples without the risk of breaking

the tube. This design solved the problem of having to break the vessel but was also not an ideal concept. The volume would be much bigger than the closed vessel. The seals need to be tight on the glass so that the gas does not leak out, however this makes removing the fittings difficult and one would be likely to accidently break the tube at some point.

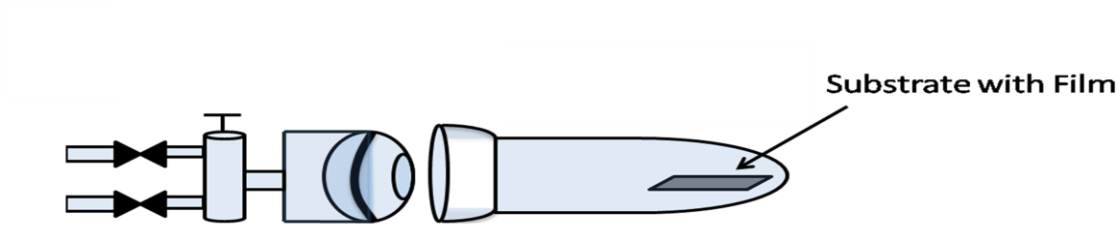

Figure 2.4: Quartz Tube Concept

The stainless steel concept takes a similar design of quartz concept 2 in that the basic idea relies on the use of a long narrow chamber attached to gas inlets. The stainless steel design is comprised of a long rectangular section which is closed at one end while the other is attached to a square gas inlet pocket. A rubber mat would be cut to the inner area of the square and a slot left for gas to flow into the chamber. A cap with gas fittings would then be fit and screwed into the square pocket. The cap will press against the rubber gasket creating and airtight seal. The stainless steel benefits from the quartz designs in that it is simpler in design and is much less expensive. The rectangle chamber also creates a much smaller volume than the round tube of the quartz tube concept. Potential drawbacks arise from the material properties of stainless steel. Stainless steel is much heavier than quartz and would require supports so that the furnace does not bear all of the chambers weight. There is also a

question of thermal stresses along the chamber. As will be seen in the next section, parts of the chamber will be outside of the furnace and must be cooled so that the rubber gasket does not melt. This may cause stresses that could potentially crack the chamber welds, especially over multiple experiments. Perhaps the most major concern is that impurities in the stainless steel may leach out and contaminate the sample.

All things being considered, the stainless steel concept was chosen for the final design mainly for its mechanical stability and cost. The contamination issue will be addressed by heating the chamber to 800°C which will hopefully bleed off any materials that may be released upon heating. The final concept has three ports. One port hooks up the gas tank/vacuum pump, one will allow for a thermocouple to be place in the chamber to measure sample temperature, and one will be fitted with a bleed valve that will ensure that the chamber pressure does not surpass the ambient pressure. The final design can be seen in figure 2.5 and the full setup will be discussed in more detail below.

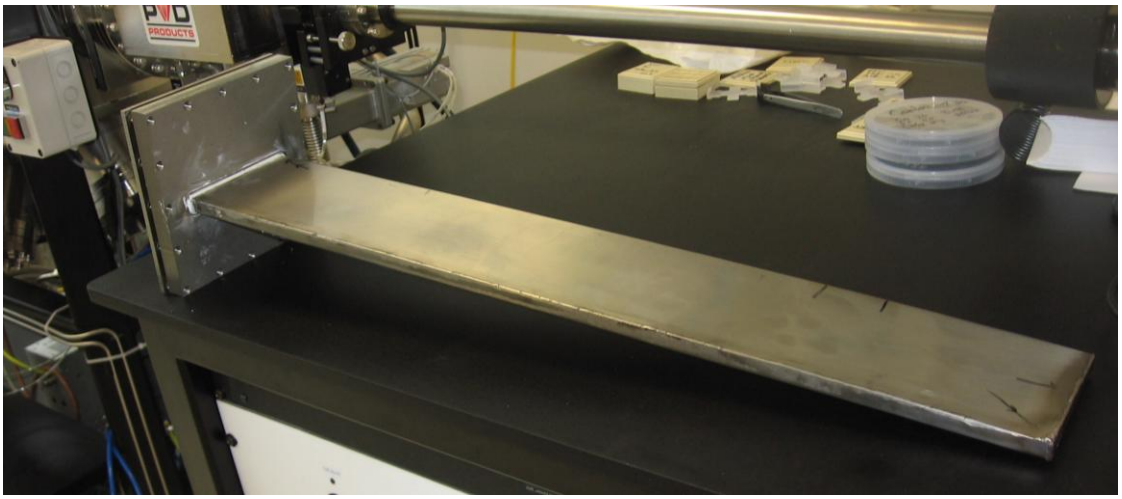

Figure 2.5: Diffusion Chamber

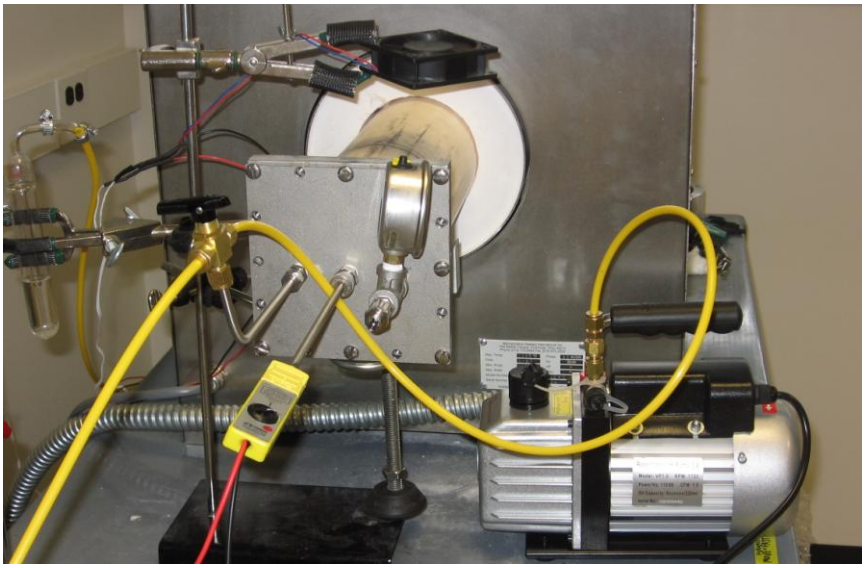

Figure 2.6: Chamber in Furnace

2.3.3 Oxygen Exchange Setup

The combinatorial film was placed into the rectangular portion of the chamber then slid down to the opposing end. The end cap is screwed on and the chamber is placed into the furnace. The first major step is to ensure that the combinatorial film is oxygen dense and free of impurities. This is done by annealing the sample at 400°C in a 20 to 80 99% pure ^{16}O gas to air mix for 5 minutes. This ensures that the oxygen in the perovskite structure is ^{16}O and helps to get rid of any impurities that might be in the crystal structure. This initial anneal also helps to produce more accurate SIMS testing as it gives reasonable confidence that there are no oxygen isotopes in the oxide film.

Future work involves the ^{18}O exchange. By using known D (bulk diffusion coefficient) and k (surface exchange coefficient) values it was decided that these experiments should be done at 400°C. Once the sample reaches the correct temperature the chamber will be filled with 20 atom % ^{18}O mixed in air. Low atom %

was used because, as will be shown in the results section, the diffusion rate in a thin film at high temperatures for pure ^{18}O occurs too quickly for a reasonable experiment time. Lowering the concentration of ^{18}O increases the time of diffusion and allows for more accurate data. The chamber will be heated for 5 minutes at which time the vacuum pump will be engaged so that no more diffusion can take place. Once cool, the sample will be taken out of the chamber and SIMS will be performed. A diagram of the furnace system is shown in figure 2.7. The system has been constructed and can be seen in the appendix, however the ^{18}O experiments have not been performed.

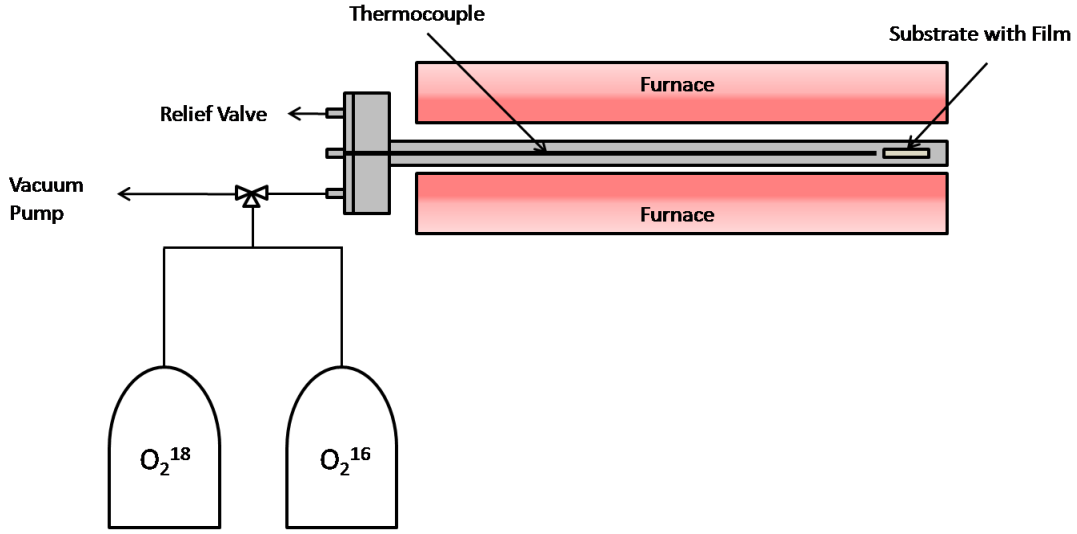

Figure 2.7: Furnace Diagram

2.4 Secondary Ion Mass Spectrometry

SIMS is a characterization technique which can measure the atomic composition of very thin materials or the surface of bulk materials. During SIMS analysis, an ion beam is shot at the sample. The ions collide with the surface causing the atoms of the sample to escape. The released surface atoms are then measured by a mass analyzer. Because SIMS measures mass, this method can differentiate different

isotopes of the same element. The one negative aspect of SIMS is that during the ion beam collision, the sample is essentially destroyed and cannot be reused for further experimentation. The technique's ability to analyze very small thicknesses makes it a very convenient method for measuring the compositions of the combinatorial thin films. (Kilner 1984) For a full oxygen diffusion study SIMS will be used in two ways. In this study, SIMS will be used to measure the composition of the films with respect to La, Sr, and Co concentrations. These values will map out the substrate and verifies what compositions are being studied. In future work, SIMS will be used after the oxygen isotope exchange to measure the depth that ^{18}O was able to travel in a specified amount of time. These values will give enough data to solve the diffusion equation.

2.5 Diffusion Equation

The end goal of this study is to provide a method by which one can ultimately find the surface exchange coefficient k and bulk diffusion coefficient D for oxygen. These values can be solved simultaneously using the diffusion equation for a semi-infinite solid. While the diffusion coefficients were not solved for in this study, an outline for future work is provided on how to do so. The strategy to measure oxygen diffusion through the film will focus on isotope exchange. While 99.76% of oxygen is ^{16}O, there are small amounts of isotopes found in nature, specifically ^{18}O. ^{18}O diffuses in the same way as the more common oxygen and therefore it is possible to measure diffusion by measuring the depth that ^{18}O can penetrate the sample over a specified time. This is possible because SIMS (being a mass measuring technique) can differentiate between isotopes and therefore the depth of ^{18}O diffusion can be measured. The depth that the ^{18}O reaches in a given time will allow the values of D

and k to be solved. The derivation is described in detail in Kilner 1996 and will be used in this study.

Total surface flux in and out of ^{18}O is measured by subtracting flux in by flux out and is represented by $J_O^{in}C_g - J_O^{out}C_s$ where C_g is the isotope ratio of the gas and C_s is the isotope ratio of the surface. At equilibrium $J_O^{in}=J_O^{out}=J_O$ and reduces surface the surface flux equation to $J_O(C_g-C_s)$. At x=0 the total flux is equal to the diffusional flux and leads to the following equation:

$$J_O(C_g - C_s) = -D[O]\frac{\partial C(x)}{\partial x} \tag{2.1}$$

Where [O] represents the total oxygen concentration and C(x) is the molar fraction of $^{18}O=\frac{N(18)}{N(18)+N(16)}$. k can be written as $\frac{J_O}{[O]}$ and so the equation 2.1 simplifies to :

$$k(C_g - C_s) = -D\frac{\partial C(x)}{\partial x} \tag{2.2}$$

The differential equation for diffusion into a semi-infinite plane has been previously solved by Crank and yields the final diffusion equation:

$$\frac{C_x - C_{bg}}{C_g - C_{bg}} = \operatorname{erfc}\left(\frac{x}{2\sqrt{D*t}}\right) - \exp\left(\frac{k*x}{D} + \frac{k^2*t}{D}\right) * \operatorname{erfc}\left[\left(\frac{x}{2\sqrt{D*t}}\right) + \left(\frac{k}{D}\sqrt{D*t}\right)\right] \tag{2.3}$$

Equation 2.3 will be used both for the initial mathematical modeling as well as for the final measurements of D and k after testing.

Chapter 3

RESULTS

3.1 Crystal Structure Characterization

Controlling the crystal structure was one of the key aspects to ensure successful results. Solid oxide fuel cell cathodes are exclusively made from materials with the perovskite crystal structure. As discussed earlier, perovskite structures have thermal and electrical properties which make them ideal for many applications. In this case, the base material is $LaCoO_3$ with a perovskite crystal structure which is then doped with Sr. The Sr occupies an A site which causes a charge imbalance and leads to the formation of oxygen vacancies. At elevated temperatures, the vacancies allow oxygen to travel freely throughout the material. For these reasons this study requires that all of the sputtering targets be of the perovskite crystal structure so that the combinatorial film will also be composed of a perovskite structure. This helps to validate that the results found are representative of real world SOFC cathodes.

X-ray diffraction (XRD) was used to confirm the crystal structure of the sputtering targets. In this method, x-rays are shot at the calcined powder of one the targets. The x-rays travel through the powder until they collide with atoms in the lattice and bounce off. The x-rays will bounce of each layer of the crystal structure to produce data for that specific crystal structure. The results of this data can be seen in figure 3.1.

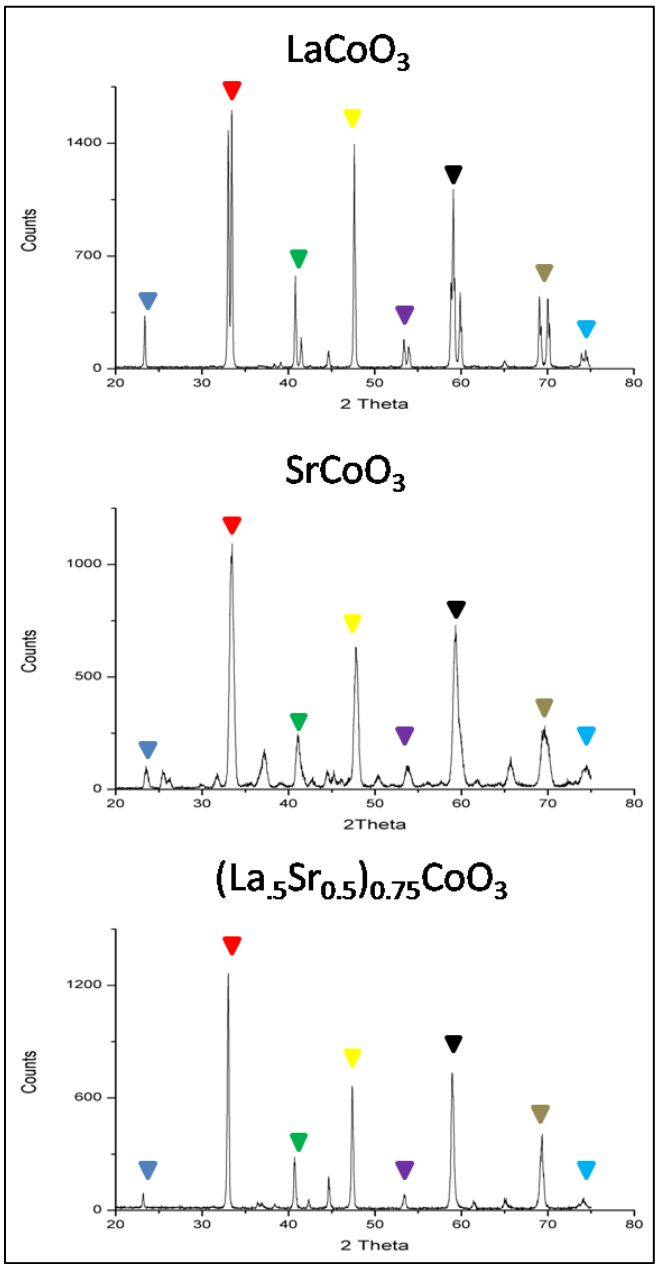

Figure 3.1: X-ray diffraction patterns of the three target materials. Triangles indicated expected peak positions for the perovskite crystal structure

Once the XRD results were found, the peaks were analyzed to assure that the proper perovskite phase had been reached. This was done by first comparing the three graphs to one another. X-ray diffraction peaks are used to find the crystal structure of materials, therefore the graphs are independent of the material being examined. As all of the target material is desired to be perovskite, their diffraction patterns should be the same. In figure 3.1, the arrows indicate similar diffraction peaks which confirm that all of the target materials were of the same phase. The diffraction patterns were then cross referenced with XRD studies of perovskite materials in Laberty-Robert 2004. It was found that the diffraction patterns matched well with the literature. The shorter diffraction peaks represent other phases, however the concentration of these phases is small especially in comparison with perovskite phase and should not significantly affect the oxygen diffusion results. For comparison, the XRD pattern of an uncalcined multiphase $(La_{0.5}Sr_{0.5})_{0.75}CoO_3$ can be found in the appendix.

3.2 Deposition Rates

Deposition rates were measured at a variety of operating conditions. As discussed earlier the three variables that were altered in the sputtering were the operating pressure, argon to oxygen ratio, and the gun power. The deposition was measured by taping half of three 10 cm x 10 cm silicon substrates then sputtering for 3 hours at a constant rotation. Once the samples were sputtered the tape was removed and the samples were resputtered with titanium for one hour. The titanium is needed because interferometry was used to measure the step height. Interferometry uses reflected light to measure differences in height and it was found that, at small heights, the step change could only be measured if they had a layer of reflective titanium over

them. An example of the interferometry surface analysis can be seen in figure 3.2. Deposition rate data can be seen in figures 3.3 and 3.4. In addition, two sets of operating conditions were measured using 8 samples and without rotation so that the height profile with respect to distance could be found. The results were then interpolated to find a general relationship between distance and deposition height. This data can be found in figures 3.5-3.8.

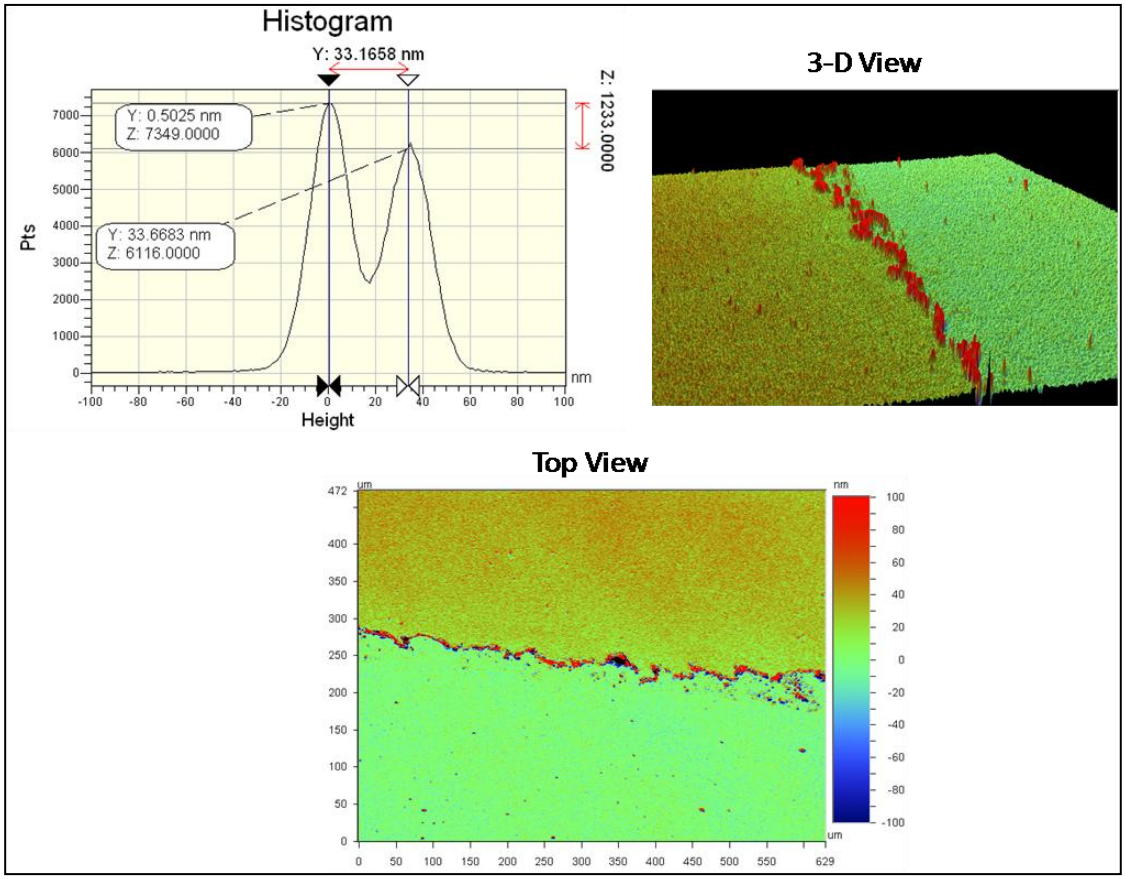

Figure 3.2: $SrCoO_3$ step measured by interferometer. Top and 3-D view show step function. Histogram shows how many points correspond to a specific height. The peaks represent the difference between steps.

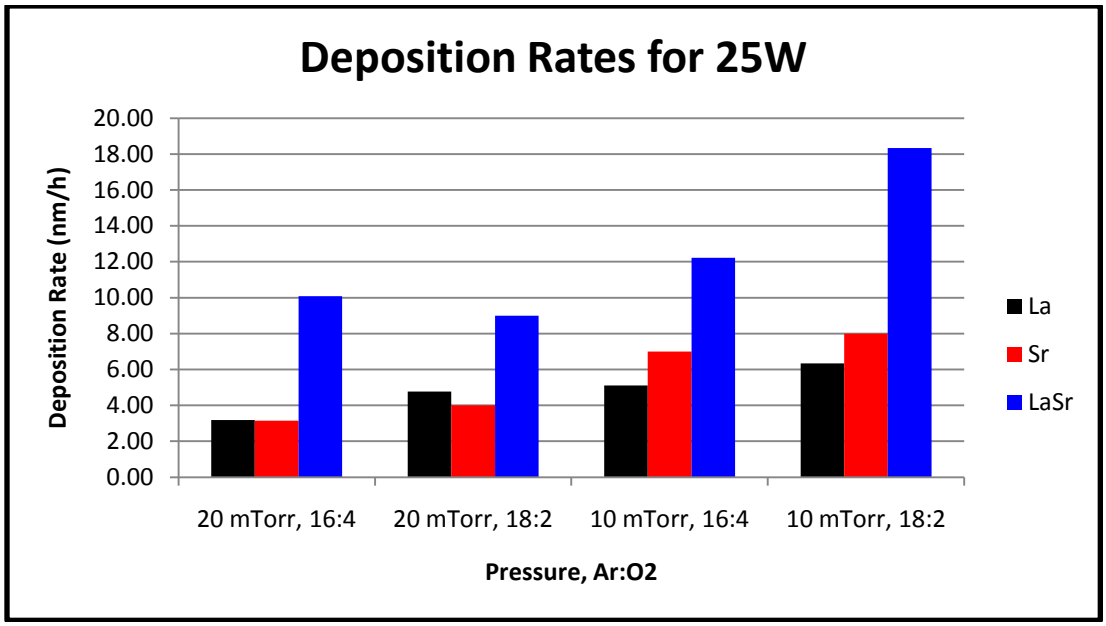

Figure 3.3: Deposition Rates at 25 Watts

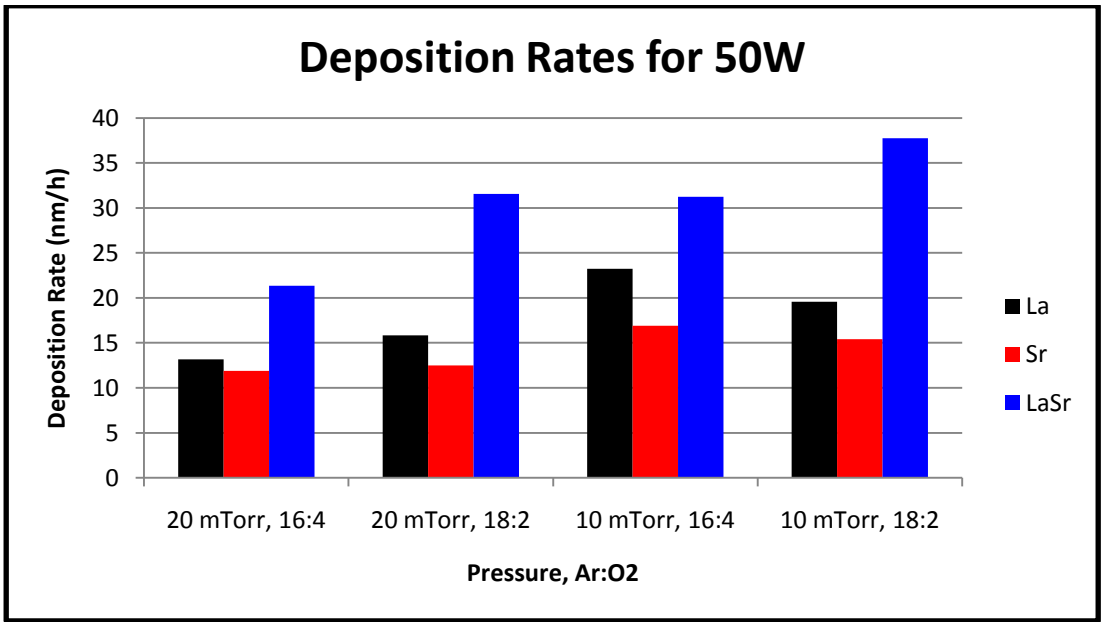

Figure 3.4: Deposition Rates at 50 Watts

By comparing the data one can see that the power is linearly proportional with the deposition rate. Decreasing the operating pressure from 20 to 10 mTorr increased deposition rate 30-40%. Changing the gas composition increased the deposition rate by 0-5% in the $LaCoO_3$ and $SrCoO_3$ (the samples in the RF guns) and up to 20% in the mixed LaSr target (DC gun). DC power is known to have higher deposition rates than their RF counterparts. Decreasing the operating pressure increases the mean free path of the atoms and allowed for a jump in deposition rate. Increasing the argon in the gas ratio also lead to minor improvements however it seems as if the increase from 16 to 18 was not significant enough to increase the deposition rate of the targets in the weaker RF guns.

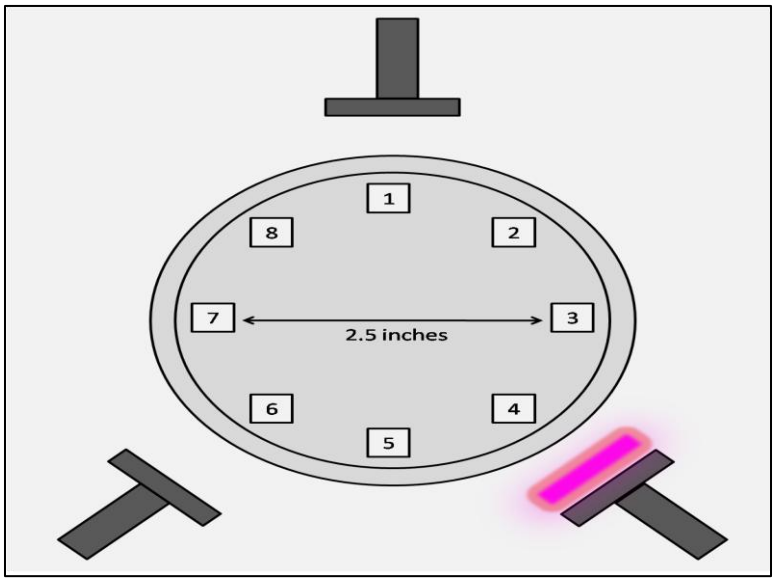

Figure 3.5: Setup for non-rotated sample to measure deposition rate relative to position from sputtering gun

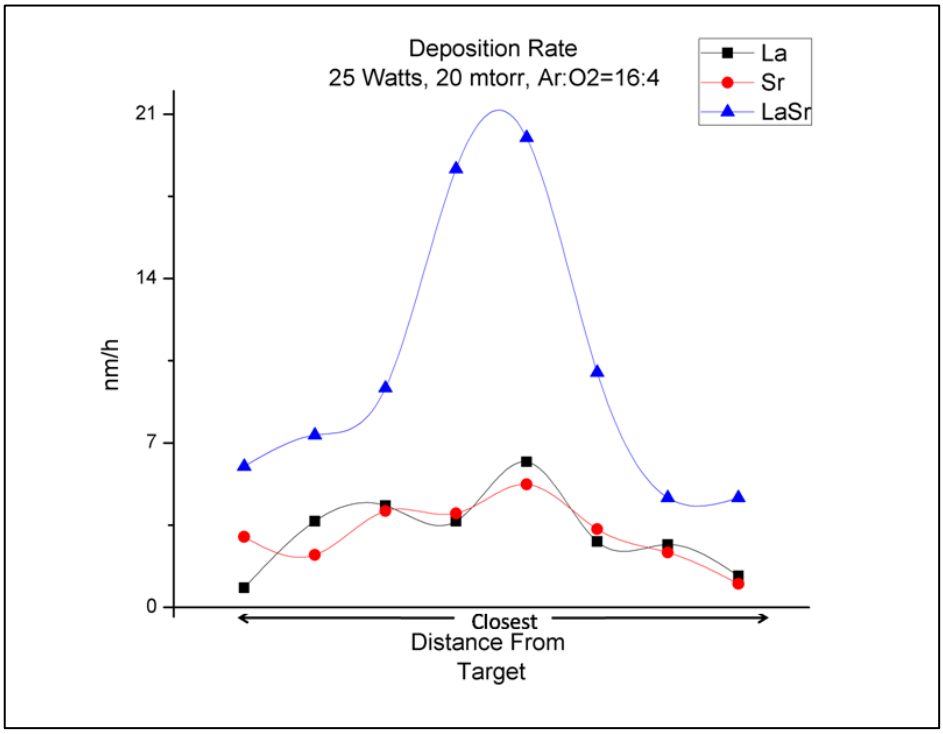

Figure 3.6: Deposition Rate in Relation to Distance from Target for 25 Watts

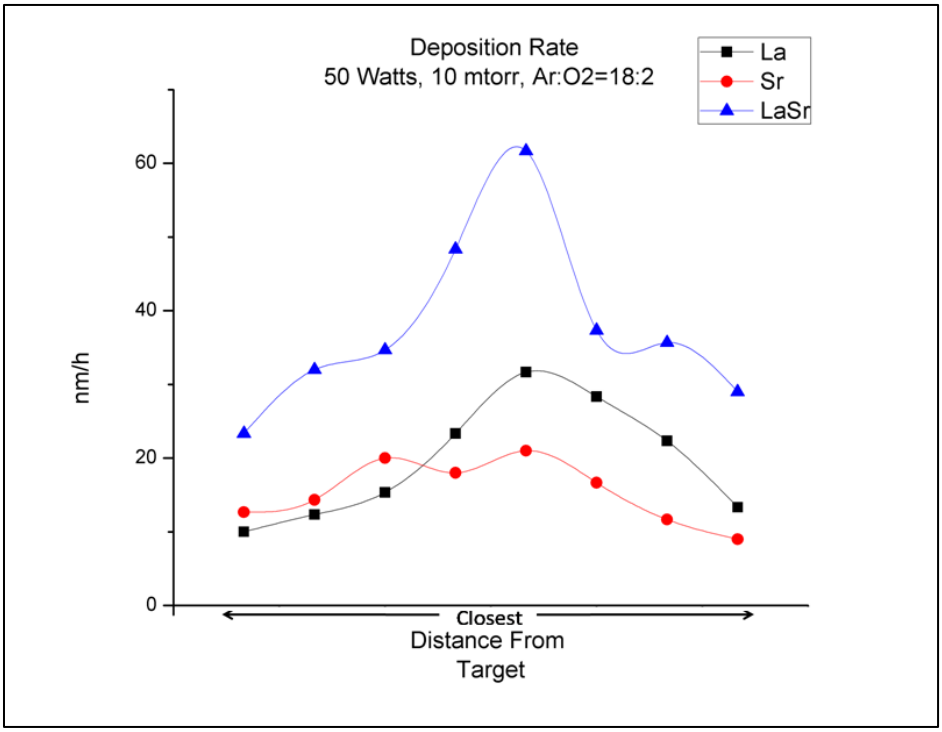

Figure 3.7: Deposition Rate in Relation to Distance from Target for 50 Watts

The distribution graphs show a fairly uniform distribution. Figures 3.6 and 3.7 show how the deposition rate varies around the substrate at eight points. This data was then used to interpolate the deposition of the interior points. The graphical representation gives a good basis for changing the sputtering settings to create combinatorial films of specific compositions.

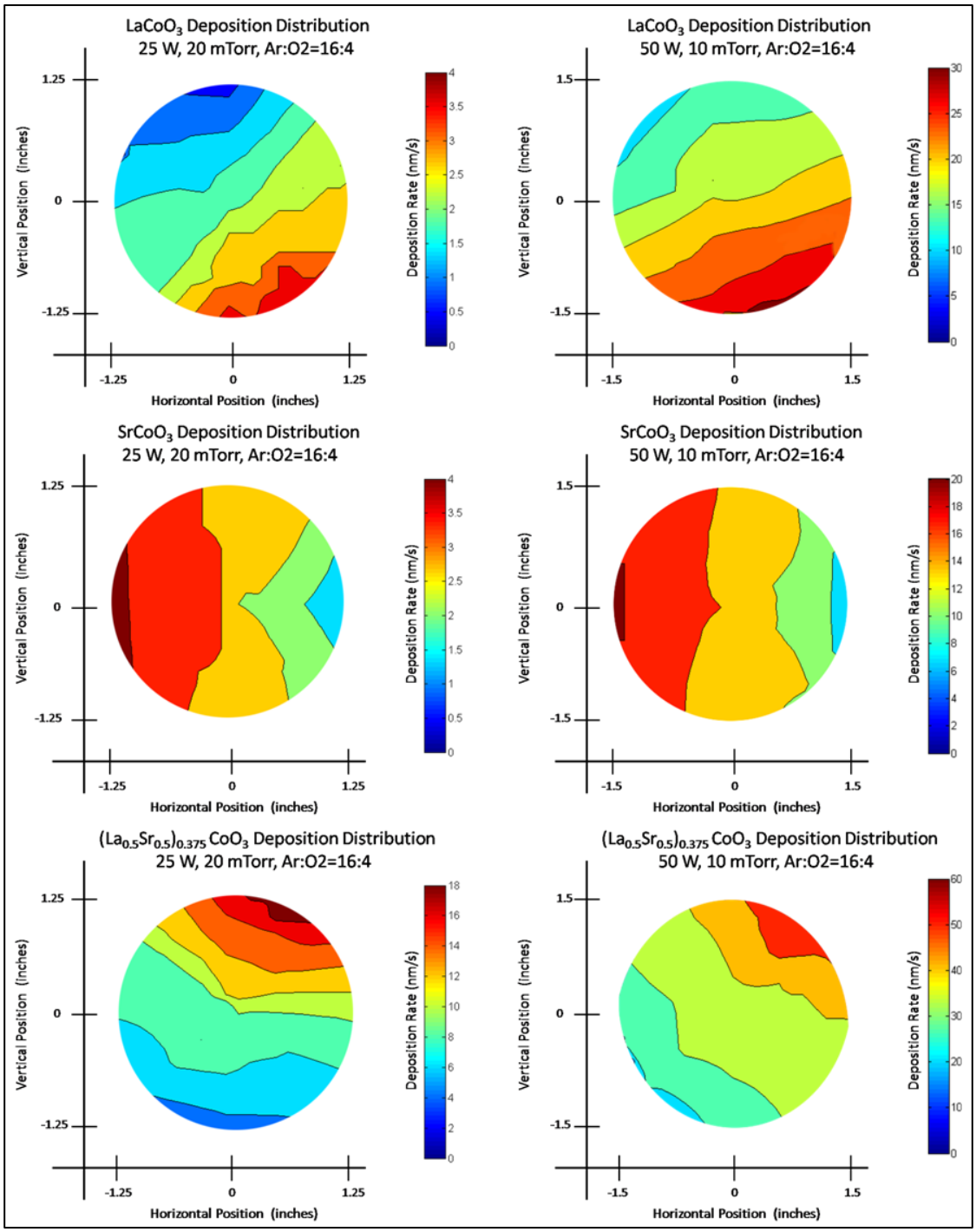

Figure 3.8: Interpolated Deposition based on data from figures 3.6 & 3.7

3.4 Compositional Measurement

An initial combinatorial film was created using the same sputtering power on all three targets. The conditions for deposition for this film was [Ar:O_2 =16:4, pressure= 10 mTorr, power=25 W, time 3 hours]. This film was then characterized using SIMS. The initial results show the concentration of La, Sr, and Co. Measurements were taken in a triangular pattern with each corner corresponding to one of the three targets.

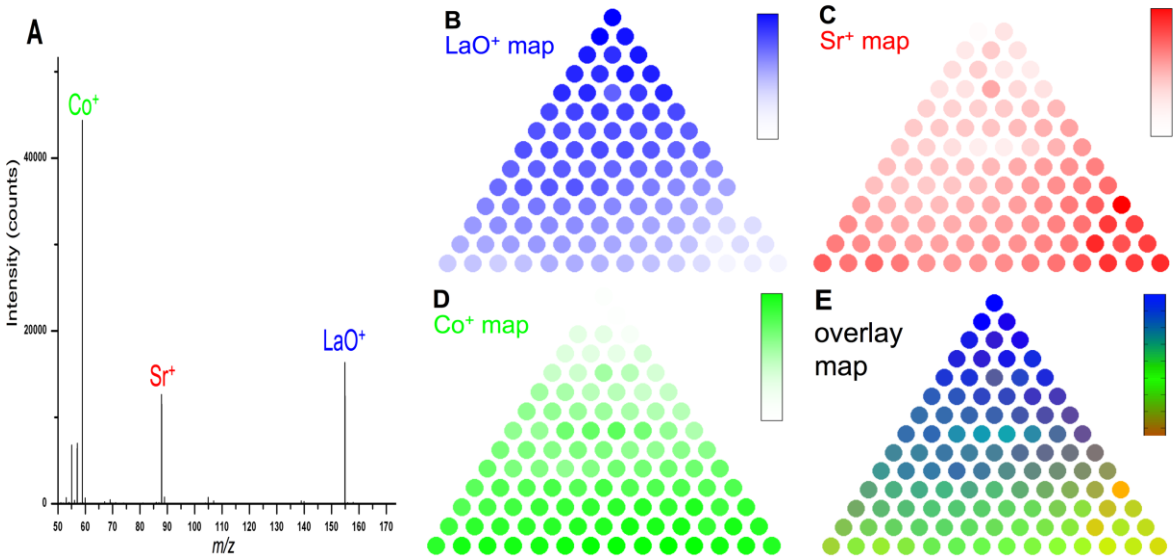

Figure 3.8: SIMS Compositional Measurement

The film in figure 3.8 was made using equal powers of 25 W for all targets. As can be seen by 3.8A, the intensity of Sr^+ and LaO^+ are similar and therefore can be inferred that there is a large distribution of compositions throughout the film. Co^+ is much higher which is expected because each sputter target contained a cobalt component.

The SIMS measurement data shows that an acceptable combinatorial film was fabricated.

While the initial film shows promise, there are several issues that need to be addressed. The first is that the Co concentration decreases unexpectedly in the top corner. Also, the Sr, concentration seems to increase in the bottom right extreme corner where it is expected to be less prevalent. For these reasons, a set of more optimal films has now been made using different powers on each target so that the deposition rates are approximately equal. The conditions for the new set of films were[$Ar:O_2$ =16:4, pressure= 10 mTorr, power La=36 W, power Sr=50 W, power LaSr=27 W, time 30 hours] which will result in an estimated thickness of 1.5 microns.

3.5 Preliminary Computational Results and Experimental Limitations

As previously stated, the diffusion equation for a semi-infinite solid will be a major tool to produce D and k values after the oxygen isotope exchange. There has been no study of thin film ceramic oxygen diffusivity on $(La_{1-x}\,Sr_x)_{1-y}CoO_3$, thereby making it difficult to predict exactly how quickly oxygen will pass through such a small layer and how much different annealing temperatures affect the diffusion time. Diffusion coefficients for bulk $La_{0.8}Sr_{0.2}CoO_3$ and $La_{0.5}Sr_{0.5}CoO_3$ have been studied. Values of these materials from DeSouza 1998 were used to approximate the amount of time, temperature, and what thickness the films needed to be for a reasonable experiment. Figure 3.9 illustrates the depth of diffusion at a specified time t. In this case, 5 minutes was used to serve as a reasonable time for the annealing process. This initial graph is similar to what SIMS will produce which will give all variables in the diffusion equation except for D and k. Figure 3.10 and 3.11 are somewhat reciprocal graphs of one another. In figure 3.10, depth is held constant at 2

microns while in figure 3.11 time is held constant at 60 seconds. These two graphs are intended to show how the diffusion rate is significantly increased with increased temperatures. In the graphs 3.10 and 3.11, the depth and time given are when the ratio of the C_x to C_{bg} is equal to 0.01. At this ratio, the ^{18}O composition in the film can be approximated to be the same as ambient conditions, meaning that at a 0.01 ratio represents the deepest depth the ^{18}O traveled through the film.

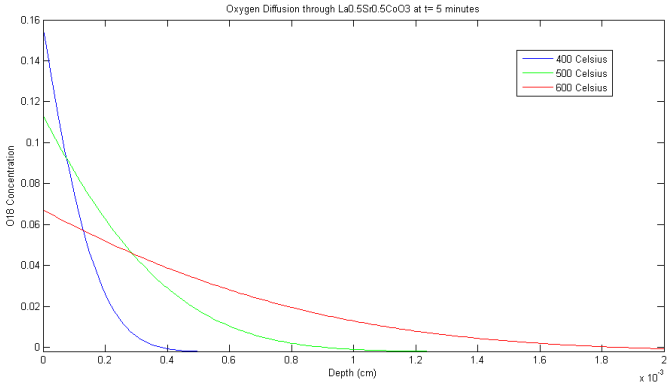

Figure 3.9: Diffusion of ^{18}O to background at t= 5 min.

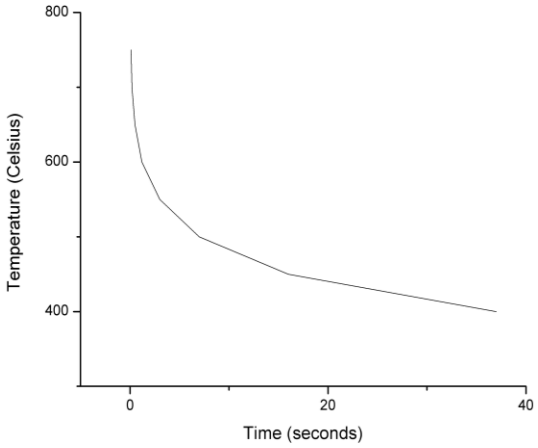

Figures 3.10: Time of Diffusion vs. Temperature for 2 Micron Depth

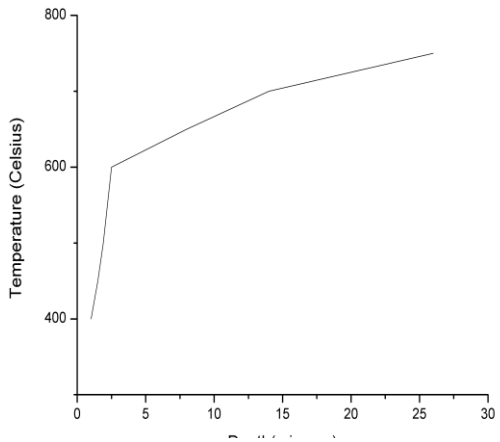

Figure 3.11: Depth of Diffusion vs. Temperature for 60 Seconds

These preliminary graphs using k and D values from the literature serve as the basis for the initial oxygen exchange experiments. As the nature of this study is the characterization of thin films, slower diffusion times are necessary so that a proper depth profile can be reached without saturating the entire film with ^{18}O. A temperature of 400°C is the lowest temperature that k and D values were found in the literature. This yielded diffusion depth of about 4 microns. This depth can be decreased in two ways. The first is to decrease the temperature. This will slow down the diffusion process and allow for thinner films to be used. The other way is to lower the amount of time that the diffusion reaction takes place. In this circumstance, this is not a desirable in that the graph is already showing a low diffusion time of 5 minutes. As time decreases, the error associated with measuring said time increases. Therefore, an annealing time of at least 5 minutes is recommended. An interesting feature to note about figure 3.9 is that while the gas atmosphere is 20 atom % oxygen, the composition at the surface (x=0) is less than that ranging from 7 % to 16 %. This is

due to the high diffusivity properties of $(La_{1-x}Sr_x)_{1-y}CoO_3$. The oxygen diffuses so quickly through the solid, that in this short amount of time, the surface exchange of ^{18}O does not occur quickly enough for the surface to reach the gas concentration before the gas is cut off. This leads to diffusion curves in which the lower temperatures have a higher surface concentration after a short specified time but then the higher temperature curves overtake the lower temperature curves to yield much deeper oxygen penetration. Figures 3.10 and 3.11 show how drastically diffusion changes with increased temperatures. As temperature rises above 500°C, diffusion rate increases exponentially. It takes milliseconds for the ^{18}O gas to reach a depth of 2 microns at higher temperatures. While the oxygen isotope exchange was not conducted, this section has given information that will be useful for future work.

Chapter 4

CONCLUSIONS AND FUTURE WORK

This study has effectively created the framework whereby the oxygen diffusivity of various compositions of the same perovskite material can be tested more quickly and efficiently than traditional methods. During the first stage of research, ceramic sputtering targets were successfully made by combining multiple powders. Through XRD these targets were found to have the desired perovskite crystal structure. After the targets were made, a thorough set of experiments to measure how deposition rates were performed. The deposition rate experiments tested three compositional targets with varying operating conditions. This was done by measuring the step height after three hours of deposition by interferometry. After deposition rates were measured, a combinatorial film was fabricated. SIMS was then used to measure the composition of the films which was shown to contain various compositions of $(La_{1-x}\,Sr_x)_{1-y}CoO_3$. Unfortunately, due to time constraints, the final phase of the project (oxygen isotope exchange) could not be completed. These experiments should be completed within the next month upon which time the study will reach completion.

This work was successful in creating the foundation for a new testing method for diffusion measurements in perovskite materials and is an effective method for optimization experiments when a preferred composition is not known. Due to the high amount of applications associated with perovskite materials, the impact of this study can reach far beyond the field of energy technologies and should be helpful to much of the research involved with perovskite materials.

APPENDIX

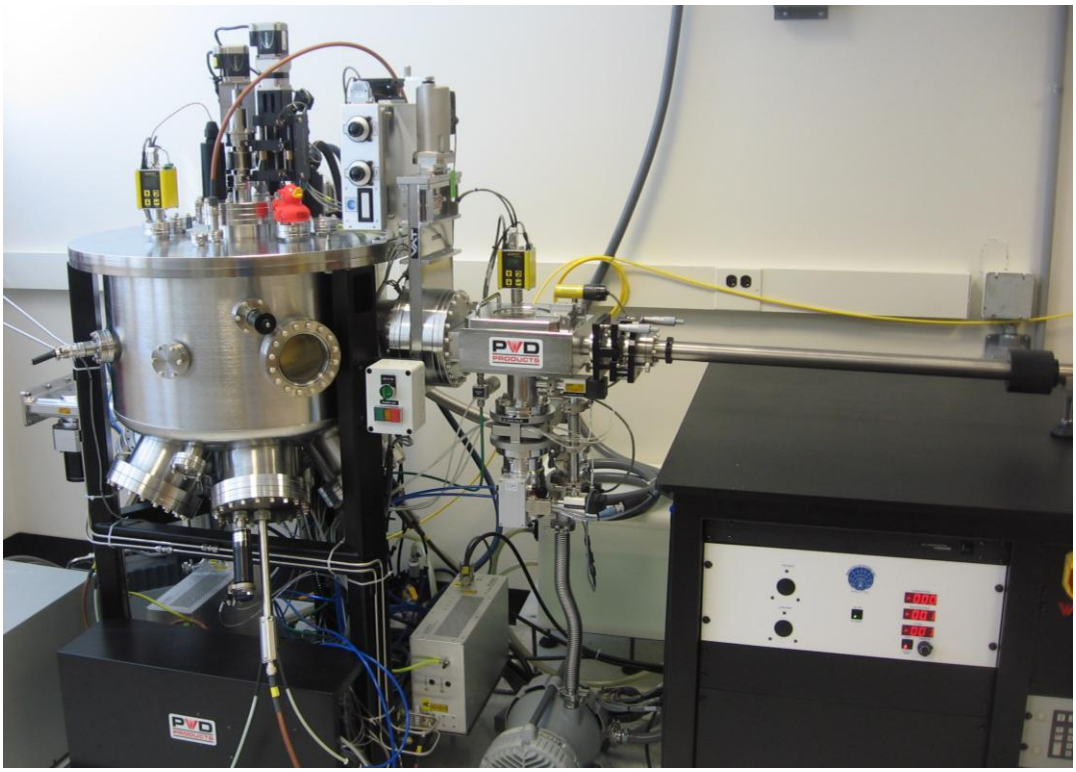

Figure A-1: PVD Sputtering Machine

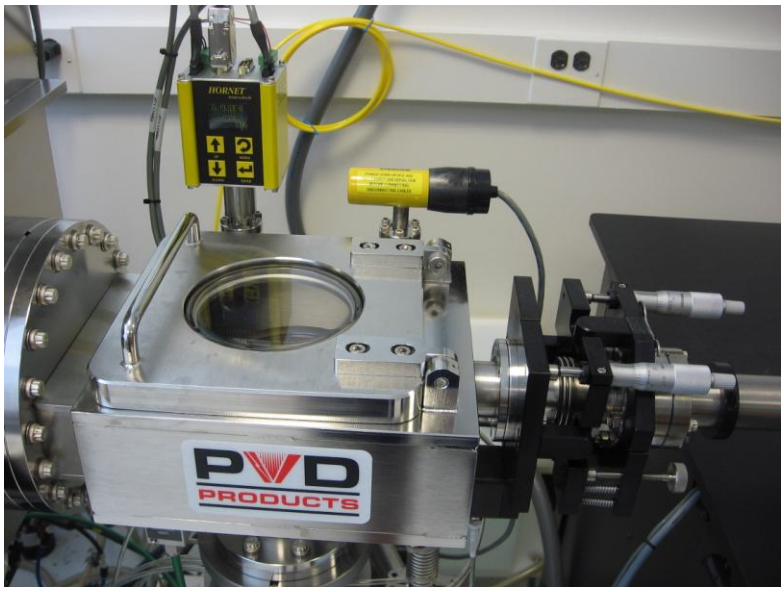

Figure A-2: Sputter Machine Loadlock

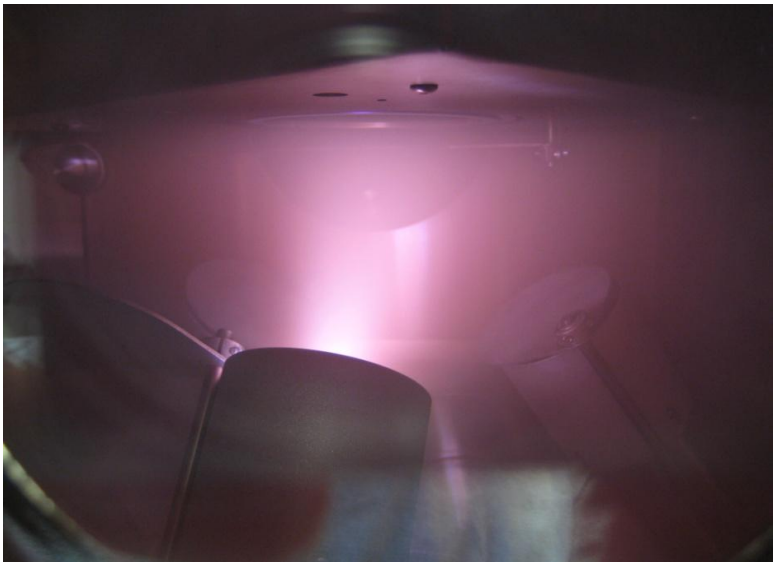

Figure A-3: Plasma Sputtering

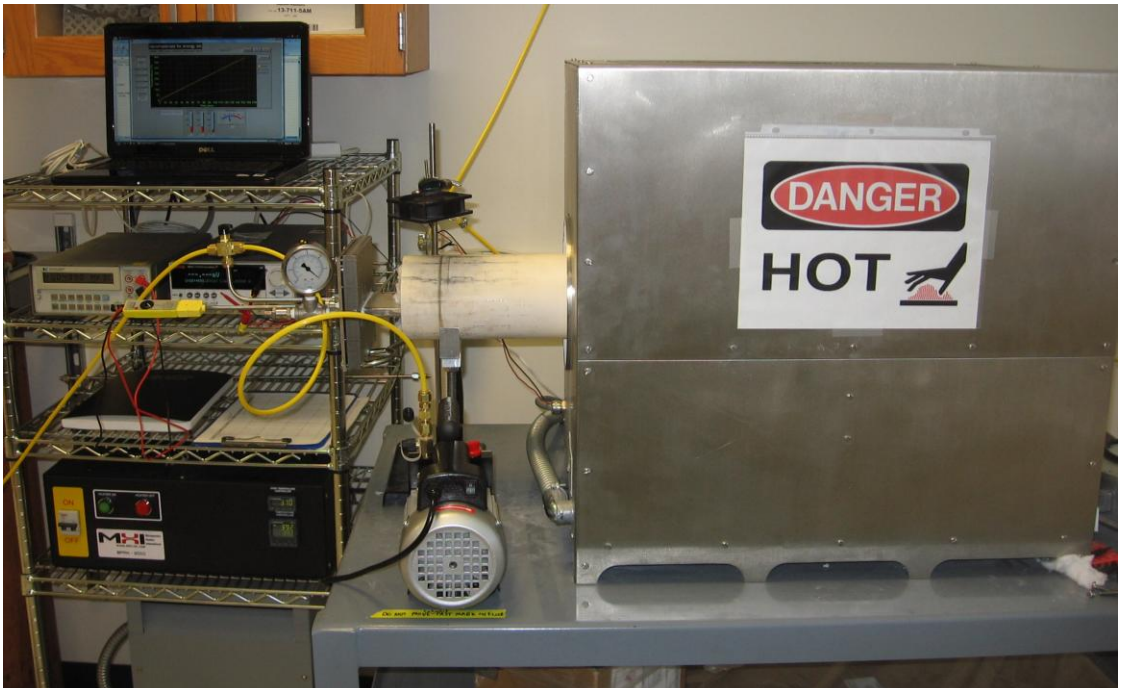

Figure A-4: Furnace

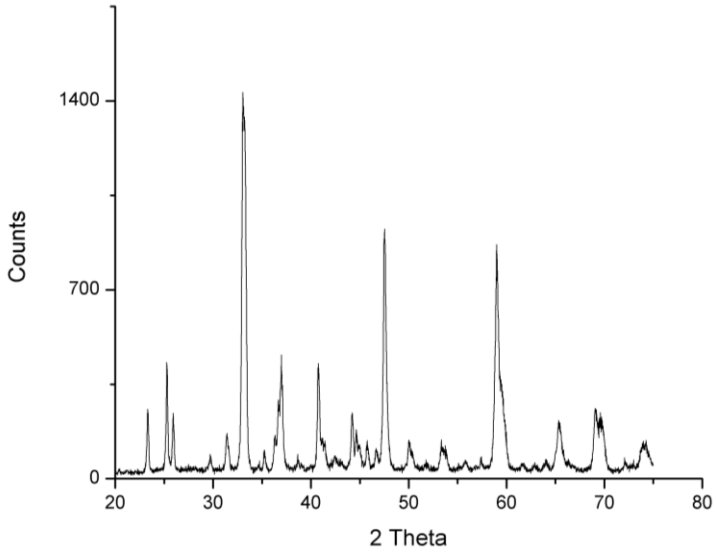

Figure A-5: Multiphase $(La_{0.5}Sr_{0.5})_{0.75}CoO_3$

References

Tatsumi Ishihara, John A. Kilner, Miho Honda, Natsuko Sakai, Harumi Yokokawa, Yusaku Takita, Oxygen surface exchange and diffusion in LaGaO3 based perovskite type oxides, Solid State Ionics, Volumes 113-115, 1 December 1998, Pages 593-600

J. A. Kilner, R. A. De Souza, I. C. Fullarton. Surface exchange of oxygen in mixed conducting perovskite oxides. Solid State Ionics, Volumes 86-88, Part 2, July 1996, Pages 703-709

J.A. Kilner, B.C.H. Steele, L. Ilkov. Oxygen self-diffusion studies using negative-ion secondary ion mass spectrometry (SIMS). Solid State Ionics, Volume 12, March 1984, Pages 89-97

Haruo Kishimoto, Natsuko Sakai, Teruhisa Horita, Katsuhiko Yamaji, Manuel E. Brito, Harumi Yokokawa, Cation transport behavior in SOFC cathode materials of La0.8Sr0.2CoO3 and La0.8Sr0.2FeO3 with perovskite structure, Solid State Ionics, Volume 178, Issues 21-22, 31 July 2007, Pages 1317-1325

James Larminie and Andrew Dicks. Fuel Cell Systems Explained. West Sussex: JohnWiley and Sons Ltd., 2006

P.J. Meier and G. L. Kulcinski.2000. Energy Payback Ratio and CO2 Emission Associated with Electricity Generation from a Natural Gas Power Plant. Proc. of Third Annual Research Highlights Forum, UW-Madison and Energy Center of Wisconsin, Madison.

Nguyen Q. Minh.J.Am. Ceramic Fuel Cells. Ceramic Soc. 76(3) 563-88(1003)

Jeremy C.H. Rossiny, Jennifer Julis, Sarah Fearn, John A. Kilner, Yong Zhang, Lifeng Chen, Shoufeng Yang, Julian R.G. Evans. Combinatorial characterization of mixed conducting perovskites. Solid State Ionics, Volume 179, Issues 21-26, 15 September 2008, Pages 1085-1089

J.C.H. Rossiny, S. Fearn, J.A. Kilner, Y. Zhang, L. Chen. Combinatorial searching for novel mixed conductors Solid State Ionics, Volume 177, Issues 19-25, 15 October 2006, Pages 1789-1794

University of Cambridge. Ferroelectric Materials. http://www.doitpoms.ac.uk/tlplib/ferroelectrics/printall.php?question=4&type=1. 2010